Predissociation of H_2 in the $3p\pi D\ ^1\Pi_u^+$ state

Hong Gao and Christian Jungen
Laboratoire Aimé-Cotton, Centre National de la Recherche Scientifique, Université de Paris–Sud, 91405 Orsay, France

Chris H. Greene
Department of Physics and Joint Institute for Laboratory Astrophysics, University of Colorado, Boulder, Colorado 80309
(Received 4 January 1993)

A noniterative eigenchannel R-matrix approach, combined with the quantum-defect method, is formulated to describe the predissociation of H_2 in the Rydberg state $3p\pi D\ ^1\Pi_u^+$ by the low-lying $3p\sigma B'\ ^1\Sigma_u^+$ and $2p\pi C\ ^1\Pi_u^+$ states belonging to the same Rydberg channel. The Coriolis coupling leading to the dissociation has been accounted for by a rovibrational frame transformation. The predissociation line positions and widths for the $v=3$ to $v=11$ levels have been calculated. Very good agreement between experiment and theory is obtained.

PACS number(s): 33.10.Cs, 33.10.Lb, 33.80.Gj, 34.80.Kw

I. INTRODUCTION

Much of the complexity of an excited molecular system derives from the coupling of electronic and nuclear degrees of freedom. These correlations give rise to multiple decay paths for the system. The most interesting spectroscopic region is where the basic molecular deexcitation processes, namely, fluorescence, ionization, and dissociation, are in strong competition [1,2]. Besides, related processes such as dissociative recombination and associative ionization also occur in this energy range [3,4]. Understanding how electronic and nuclear coupling mediate the decay of the system into such different escape channels is a very general problem. The hydrogen molecule is a prototype molecule which has been subjected to both experimental [5–7] and theoretical [8–11] studies. The simplicity of the system enables one to explore the complicated coupling of electronic and nuclear motion in great detail.

Among numerous theoretical approaches, the multichannel quantum-defect theory (MQDT) [12,13] provides one of the most powerful methods to describe these nonadiabatic effects. The role of rovibronic coupling in the ionization processes has been well documented in terms of the MQDT [8]. It has been shown that a Born-Oppenheimer quantum-defect function contains all the necessary information about the short-range electronic-nuclear coupling. The non-Born-Oppenheimer effects which occur typically in Rydberg states (large electron-core distances) can be accounted for by a quantum-mechanical basis transformation from the molecular to the laboratory frame [14]. It has thus been possible to describe the interconversion of energy between rovibronic and electronic degrees of freedom in the preionization of H_2 [13].

There have previously been mainly two types of theory which aim at including dissociative processes in the MQDT framework. First, Giusti-Suzor [15] developed a perturbative treatment of competing ionization and dissociation processes. In this method a second body-frame interaction parameter is introduced, in addition to the quantum-defect function, to account for the electronic coupling between the Rydberg and dissociative valence states. This coupling is then treated perturbatively to lower orders. This method has been successfully applied to describe dissociative recombination and associative ionization processes for several molecules (H_2, O_2, and Na_2) [3] in which the electronic coupling is only moderately strong. However, it encounters convergence problems in the case of strong coupling.

Somewhat later one of us proposed a nonperturbative eigenchannel R-matrix method to explain how the ionization and the dissociation compete in H_2 photoabsorption [2]. It has been shown that the same quantum-defect function as used in the ionization processes also contains the necessary information to deal with dissociation. This treatment is thus formulated in terms of exactly the same parameters as those used in the MQDT of rovibronic coupling in molecular Rydberg states [8]. Although this approach is accurate, it involves determining iteratively at a given total energy a complete set of short-range eigenstates, each of which has a constant eigenphase in both ionization and dissociation channels. This iteration procedure has thus been shown to be difficult to implement in numerical calculations. Robicheaux, in his treatment of H_2 vibrational excitations and dissociative attachment by electron collision [16], reformulated the R-matrix method of Greene and Jungen [17] into a noniterative version. The disadvantage of his approach, however, is that the Born-Oppenheimer approximation is assumed throughout the reaction region where the R-matrix calculation is performed. This assumption is not generally valid in dissociative processes in which the non-Born-Oppenheimer coupling may even play a role within the reaction zone.

The purpose of this work is to develop a nonperturbative approach to treat ionization and dissociation without invoking iteration. In this paper, we present the initial step towards this goal, i.e., the description of predissociation of H_2 in the $3p\pi$ Rydberg state by the lower-lying

electronic states $3p\sigma$, $2p\pi$, and $2p\sigma$ belonging to the same Rydberg channel. The rovibrational levels of this state are strongly predissociated even above the ionization threshold [7], whereas for higher $np\lambda$ ($n \geq 4$, $\lambda = 0, 1$) states ionization is dominant. Thus we neglect the ionization process entirely in the present study. Open ionization channels will be included in future studies. In what follows, we first describe the physical processes involved to give an overall view. The eigenchannel iterative treatment [2] will then be summarized. After that our noniterative formulation will be given in detail. We will finally present our results of predissociation line position and widths for the $v = 3-11$ levels of the $3p\pi D\ ^1\Pi_u^+$ ($J = 2$) state and compare them with the experimental results determined by Glass-Maujean, Breton, and Guyon [7] and the theoretical calculation of Julienne [18].

II. DESCRIPTION OF THE PROCESSES

Figure 1 shows several potential-energy curves of H_2 and that of H_2^+ relevant to our study, along with the vibrational energy levels associated with these states. These Rydberg states are members of the p-wave ionization channel which is accessible from the ground state of H_2 by absorption of one photon. Above the dissociation limit $H(1s)+H(2s,2p)$, in addition to the direct dissociation of the $2p\sigma$ (not shown in the figure), $2p\pi$, and $3p\sigma$ states, higher bound states can also be predissociated by these lower-lying members of the same Rydberg channel.

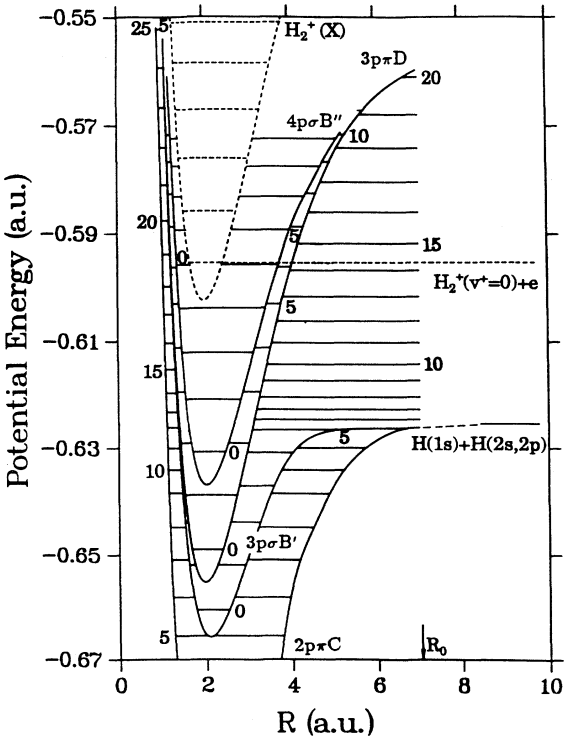

FIG. 1. Potential-energy curves of H_2 and H_2^+ relevant to this study. Also drawn are the rovibrational energy levels. These "box" levels are calculated by requiring that the wave functions vanish at R_0.

Julienne and others have shown some time ago that predissociation of the $3p\pi$ state is induced by a transition into the $3p\sigma$ vibrational continuum, caused by Coriolis interaction [18]. Herzberg [19] has further shown that a progression of typical Beutler-Fano profiles occurs in the photoabsorption cross section as a result of the interference between the direct photodissociation into the $3p\sigma B'$ state and the indirect dissociative process via the quasibound $3p\pi D$ levels v. The interaction of the $3p\pi$ state with the $2p\pi$ and $2p\sigma$ states is weaker by orders of magnitude. The reason is that all coupling occurs at short internuclear distances. The $3p\pi$ and $3p\sigma$ states approach the same electronic configuration He($3p$) in the united atom limit. The potential curves of the two states are so close to each other at short internuclear distance that they can interact very effectively [7]. The $2p\pi$ and $2p\sigma$ states, on the other hand, are so far away that their interaction with the $3p\pi$ state becomes weak. The coupling to the $2p\pi$ state is about two orders of magnitude weaker than the coupling to $3p\sigma$, while the coupling to $2p\sigma$ is even weaker and is thus neglected entirely in this calculation.

In the theoretical treatment of Julienne [18], an l-uncoupling operator $-(1/2\mu_N R^2)(J^+L^- + J^-L^+)$ is used. Here μ_N and R are the reduced nuclear mass and internuclear distance, respectively. **J** denotes the total angular momentum operator of the system. **L** refers to the total electronic angular momentum. Those with "+" and "−" are raising and lowering operators. This operator is responsible for the breakdown of the Born-Oppenheimer approximation and thus induces dissociation. The predissociation lifetime is obtained from Fermi's "golden rule" by calculating the electronic matrix elements between the initial bound state $3p\pi$ and the final continuum state $3p\sigma$ coupled by the coupling operator. This treatment, as we will see later, yields linewidths in fairly good agreement with the experimental results of Glass-Maujean, Breton, and Guyon [7], but a discrepancy still remains.

Instead of introducing an operator to treat the interaction between different states, we describe the coupling here as a channel mixing. In Rydberg states, one of the electrons is able to move far from the remaining molecular core. In this region of space, the Rydberg electron is no longer constrained to follow the rovibrational motion of the nuclei adiabatically, but instead becomes decoupled from the core motion. As a result the Born-Oppenheimer separation of electronic and nuclear motion can no longer serve as a good approximation. The good quantum numbers are now the rovibrational quantum numbers of the core and the outer-electron angular momentum quantum number [8]. Only when the electron is in the vicinity of the core will the strong interaction reassure the validity of the Born-Oppenheimer approximation.

The frame transformation [14], in conjunction with the MQDT [12,13], provides a natural framework to incorporate these nonadiabatic effects resulting from large electron-core distances. When the electron is anywhere outside the molecular core ($r \geq r_0$ with r_0 denoting the size of the core), the wave function of the system at ener-

gy E can be written as an expansion in terms of the complete set of eigenstates of the core $\phi_{v^+N^+}(\omega)$ (ω denotes all the coordinates except the radial coordinate of the outer electron r), multiplied by the outer-electron radial functions [8]

$$\psi = r^{-1} \sum_{v^+,N^+} \phi_{v^+N^+}(\omega) \times \sum_{v^{+\prime},N^{+\prime}} [f_{v^+N^+}(r) C_{v^+N^+,v^{+\prime}N^{+\prime}} - g_{v^+N^+}(r) S_{v^+N^+,v^{+\prime}N^{+\prime}}] \times B_{v^{+\prime}N^{+\prime}}, \quad r \geq r_0 , \tag{1}$$

with

$$\phi_{v^+N^+}(\omega) = \varphi^{(e)}_{\Lambda^+} \frac{\chi_{v^+N^+}(R)}{R} \Phi^{(lN^+)}_{JM}(\hat{r},\hat{R}) .$$

Here $\varphi^{(e)}_{\Lambda^+}$ is the ground electron wave function of H_2^+ (Λ^+ is the electronic angular momentum component of the core along the internuclear axis), $\chi_{v^+N^+}(R)/R$ is the vibrational wave function (with energy $E_{v^+N^+}$) in this electronic state (v^+ and N^+ denote the vibrational and rotational quantum numbers, respectively), and $\Phi^{(lN^+)}_{JM}(\hat{r},\hat{R})$ is an eigenfunction of the total angular momentum operators of the electron-core system $\mathbf{J}^2$ and $\mathbf{J}_z$ [14]. The functions (f,g) are the regular and irregular p-wave Coulomb functions evaluated at the channel energy $\epsilon_{v^+N^+} = E - E_{v^+N^+}$. The $\underline{C}$ and $\underline{S}$ matrices can be obtained by matching the laboratory-frame expansion Eq. (1) valid everywhere outside the core to the Born-Oppenheimer wave function valid in the vicinity of the core as follows [8]:

$$C_{v^+N^+,v^{+\prime}N^{+\prime}} = \sum_{\Lambda} U^{(lJ)}_{N^+\Lambda} \int \chi_{v^+N^+}(R) \cos[\pi\mu_\Lambda(R)] \times \chi_{v^{+\prime}N^{+\prime}}(R) \times dR\ U^{(lJ)}_{N^{+\prime}\Lambda} . \tag{2}$$

A similar expression holds for $\underline{S}$ with cos replaced by sin in the above expression. In Eq. (2) the coefficients $U^{(lJ)}_{N^+\Lambda}$ are the rotational frame transformation matrix elements connecting different angular momentum coupling schemes relevant at short and long range [14]. For a given electron orbital momentum l and a total angular momentum J, the matrix $\underline{U}$ has dimension $2l+1$ and it is unitary. The integration over R amounts to transforming the R-dependent body-frame quantum-defect function $\mu_\Lambda(R)$ (Λ refers to the electronic angular momentum component of the molecule along the internuclear axis) into laboratory-frame measurable quantities. The superposition coefficients $B_{v^{+\prime}N^{+\prime}}$ are chosen so that the solution in Eq. (1) satisfies the correct physical boundary conditions at large r. For a bound state, for instance, one requires that the wave function vanish at $r \to \infty$, which leads to the following linear system:

$$\sum_{v^{+\prime},N^{+\prime}} [\sin(\pi\nu_{v^+N^+}) C_{v^+N^+,v^{+\prime}N^{+\prime}} + \cos(\pi\nu_{v^+N^+}) S_{v^+N^+,v^{+\prime}N^{+\prime}}] B_{v^{+\prime}N^{+\prime}} = 0 . \tag{3}$$

Here $\nu_{v^+N^+} = Z/\sqrt{-2\epsilon_{v^+N^+}}$ is the effective principal quantum number in channel v^+N^+, and with Z the net charge of the molecular core.

The quantum defect $\mu_\Lambda(R)$ (with $\Lambda=0$ and 1 for a p channel) can be obtained either from a short-range *ab initio* calculation (within the Born-Oppenheimer approximation) or by fitting to the experimental data. This function provides sufficient information about the short-range interactions. It can be seen from Eq. (2) that channels or Rydberg series associated with different ionization thresholds ($E_{v^+N^+}$) are mixed, i.e., the off-diagonal elements $C_{v^+N^+,v^{+\prime}N^{+\prime}} \neq 0$. The R and Λ dependences of $\mu_\Lambda(R)$ are responsible for these couplings. Notice that if μ does not depend on Λ or R, the elements of Eq. (2) reduce to $\cos(\pi\mu)\delta_{v^+N^+,v^{+\prime}N^{+\prime}}$ owing to the unitarity of the $\{U\}$ and $\{\chi\}$. The rovibrational energy levels shown in Fig. 1 are calculated from the MQDT scheme [Eq. (3)]. Each one of the levels is still predominantly Born-Oppenheimer in character owing to their low principal quantum numbers, but with the coupling to all other states in the Rydberg channel included. In other words, the tedious evaluation of adiabatic and nonadiabatic correction terms like $\langle \varphi_j^{(e)} | \nabla_R^2 \varphi_i^{(e)} \rangle$ (where $|\varphi_i^{(e)}\rangle$ is the electronic eigenfunction) is avoided in MQDT, these corrections being included implicitly by solving the linear system [Eq. (3)].

III. EIGENCHANNEL R-MATRIX TREATMENT

The nonadiabatic effects arising in the large electron-core distances have been studied using MQDT in the ionization processes for some time [8]. The iterative eigenchannel R-matrix treatment [2] provides an initial attempt to include dissociation within Rydberg channels. In this approach the dissociative process is assumed to be along a well-defined Born-Oppenheimer potential curve only at large nuclear separation. This is well justified for a dissociation proceeding relatively slowly. The process in the initial stage (small internuclear distances), however, is rather complicated. One expects nonadiabatic coupling between different states due to the large nuclear velocity.

Two degrees of freedom are essential to describe the dissociation in the Rydberg channel: the distance r between the Rydberg electron and the remaining molecular core, and the internuclear distance R. The nonadiabatic effects discussed in the previous section arise to the extent that the probability amplitude of the Rydberg electron far from the core is large. Thus the higher the principal quantum number of the Rydberg state is, the stronger this class of nonadiabatic behavior will be. On the other hand, these couplings are most effective within a small-R region to induce the dissociation process. Thus the interconversion of energy between electronic and nuclear motion takes place predominantly in the small-R and large-r region.

In order to describe the complicated interaction within this reaction region, Ref. [2] defines a two-dimensional configuration space spanned by the radial coordinate r of the Rydberg electron and the internuclear distance R. An eigenchannel R-matrix calculation [20] is then set up in the reaction zone (denoted by Ω) bounded by the surfaces Σ_r ($r=r_2$ surface) and Σ_R ($R=R_0$ surface) to account for the nonadiabatic coupling. Beyond r_2 (R_0), all relevant bound electronic (vibrational) wave functions are negligible. Specifically, r_2 should be taken large enough to include not only the molecular core, but also the entire electronic state responsible for dissociation ($3p\sigma$ in this study). On the other hand, R_0 is chosen such that the relevant Born-Oppenheimer levels of the predissociating state ($3p\pi$ in this case) are well confined within this region.

The potential-energy curve and level diagram in Fig. 1 can be used to illustrate the iterative procedure of Ref. [2]. The aim of this procedure is to find for each preselected total energy E a molecular eigenstate which has a constant logarithmic derivative all over the reaction zone surface. The treatment starts by giving an arbitrary logarithmic derivative on the surface R_0 and calculating the complete set of vibrational states $\chi_{v^+N^+}(R)$ of the molecular core. One particular choice is $b(R_0)=-\chi'_{v^+N^+}/\chi_{v^+N^+}=\pm\infty$ for all v^+N^+ (where the prime refers to the derivative with respect to R). One can distinguish two types of vibrational core states. The first type consists of states which do not reach out to R_0 and are just the bound states of H_2^+; the lowest levels of this type are drawn to scale at the top of Fig. 1. The second type of levels are those extending beyond R_0 and represent a discrete subset of the H_2^+ vibrational continuum, defined by the particular logarithmic derivative chosen at R_0. These levels are off the scale of Fig. 1.

Then the multichannel expansion solution of the system at large r [Eq. (1)] can be formed by calculating the rovibrational frame transformation matrices $\underline{C}$ and $\underline{S}$ [Eq. (2)]. We consider here the particular case where all ionization channels are closed, i.e., the total energy E of the system is lower than the ionization threshold $H_2^+(v^+=0)+e$ (cf. Fig. 1). Solving the linear system Eq. (3) yields a set of eigenstates. The energy diagram in Fig. 1 is just one particular set of the eigenstates with $b=\pm\infty$, i.e., $\chi_{v^+N^+}(R_0)=0$. In general, none of the energy levels will equal the preselected total energy E. Therefore, an iteration procedure is necessary whereby the logarithmic derivative b at R_0 is varied until one of the eigenvalues coincides with E. The set of logarithmic derivatives resulting from this procedure $\{b_\beta\}$ then embodies *all* relevant information about electronic and nuclear coupling within the reaction zone $R\le R_0$ at total energy E. They are finally used to propagate the eigensolutions from the reaction zone to the asymptotic regions where the molecule is dissociated [2].

The wave function of the system at large R can be written as

$$\Psi_\beta=\sum_{n,\Lambda}\phi_{n\Lambda}[F_{n\Lambda}(R)I_{n\Lambda,\beta}-G_{n\Lambda}(R)J_{n\Lambda,\beta}]\ ,\quad R\ge R_0\ . \tag{4}$$

Here $\phi_{n\Lambda}$ denotes the dissociative electronic Born-Oppenheimer eigenstate and (F,G) are independent vibrational continuum solutions solved in this Born-Oppenheimer potential curves. The coefficients $I_{n\Lambda,\beta}$ and $J_{n\Lambda,\beta}$ can thus be obtained by connecting the above solution to the R-matrix eigenstates.

IV. NONITERATIVE EIGENCHANNEL R-MATRIX TREATMENT

In the eigenchannel R-matrix method described in the previous section one varies the logarithmic derivatives of the solution in order to find the correct values corresponding to the given total energy E. This procedure is bypassed in this work with the help of the variational eigenchannel R-matrix approach [21]. This noniterative treatment can be derived directly from the usual Ritz principle, or from Schrödinger's equation. In what follows, we first give a brief summary of the noniterative R-matrix method [21]. We will then describe our treatment using this formulation.

The well-known Ritz principle for energy can be recast in the following form using Green's theorem:

$$b(E)=\frac{\int_\Omega\left[-\frac{1}{\mu_N}\nabla_R\Psi^*\cdot\nabla_R\Psi-\frac{1}{\mu_e}\nabla_r\Psi^*\cdot\nabla_r\Psi+2\Psi^*(E-V)\Psi\right]d\omega}{\frac{1}{\mu_N}\int_{\Sigma_R}\Psi^*\Psi d\sigma_R+\frac{1}{\mu_e}\int_{\Sigma_r}\Psi^*\Psi d\sigma_r}\ , \tag{5}$$

where the parameter b is the logarithmic derivative on the reaction zone surface:

$$\left[\frac{\partial\Psi}{\partial n}+b\Psi\right]=0\ . \tag{6}$$

on Σ_r,Σ_R. In the above equations, $-\nabla_R^2/2\mu_N$ is the nuclear kinetic energy (μ_N is the reduced nuclear mass), $-\nabla_r^2/2\mu_e$ is the sum of kinetic energies of all electrons (μ_e is the mass of the electron), and V is the potential energy between all particles in the system. Ω and Σ refer to the volume and surface of the reaction zone. It can easily be shown that Eq. (5) is a variational expression for b [21].

To proceed, this treatment first represents the trial function Ψ in Eq. (5) in terms of a set of basis functions y_k:

$$\Psi=\sum_k y_k c_k\ . \tag{7}$$

Inserting Eq. (7) into Eq. (5) and applying the variational principle for b, one obtains the following generalized eigenvalue system [21]:

$$\underline{\Gamma}\mathbf{c}=b\underline{\Lambda}\mathbf{c}\ , \tag{8}$$

where the matrices $\underline{\Gamma}$ and $\underline{\Lambda}$ are given by

$$\Gamma_{kl}=2\int_\Omega y_k^*(E-H)y_l d\omega-\frac{1}{\mu_N}\int_{\Sigma_R} y_k^*\frac{\partial y_l}{\partial n}d\sigma_R$$

$$-\frac{1}{\mu_e}\int_{\Sigma_r} y_k^*\frac{\partial y_l}{\partial n}d\sigma_r\ , \tag{9a}$$

$$\Lambda_{kl}=\frac{1}{\mu_N}\int_{\Sigma_R} y_k^* y_l d\sigma_R+\frac{1}{\mu_e}\int_{\Sigma_r} y_k^* y_l d\sigma_r\ . \tag{9b}$$

The βth eigensolution $\Psi_\beta=\sum_k y_k c_{k\beta}$ from the above eigensystem thus satisfies Eq. (6) with eigenvalue b_β. It is worth mentioning that these basis functions y_k need not be orthogonal, nor must they have any particular logarithmic derivatives on the reaction zone surface. In order to obtain rapid convergence, one must include at least one basis function in each channel which has a surface logarithmic derivative different from the rest of the functions. It should also be noticed that the eigensolutions of Eq. (8) are not orthogonal over the reaction zone volume because they all have different logarithmic derivatives on the surface. Instead, they are orthogonal over the reaction zone surface, i.e., $\int_\Sigma \Psi_\beta^*\Psi_{\beta'}d\sigma=0$, since $\mathbf{c}_{\beta'}\cdot\underline{\Lambda}\mathbf{c}_{\beta'}=0$ for $b_\beta\neq b_{\beta'}$. Thus they form a complete set on the reaction zone surface on which they can be connected to the asymptotic solutions.

We next concentrate on how to construct the variational basis functions within the reaction zone. We ignore ionization in this work since the preionization of the $3p\pi$ state is negligible. The multichannel bound Rydberg wave functions in Eq. (1) provide a natural starting point. However, in order to form an eigenfunction having finite probability to extend beyond R_0, it is necessary to add basis functions of different boundary value on the surface R_0. Specifically speaking, our first class of basis functions y_i (with energies E_i) is formed in terms of the complete set of vibrational wave functions $\chi^{(1)}_{v^+N^+}(R)$ (with energies $E^{(1)}_{v^+N^+}$) determined by requiring $\chi^{(1)}_{v^+N^+}(R_0)=0$:

$$y_i(E_i)=r^{-1}\sum_{v^+,N^+}\phi^{(1)}_{v^+N^+}\times\sum_{v^{+\prime},N^{+\prime}}[f^{(1)}_{v^+N^+}C^{(1)}_{v^+N^+,v^{+\prime}N^{+\prime}}-g^{(1)}_{v^+N^+}S^{(1)}_{v^+N^+,v^{+\prime}N^{+\prime}}]\times B^{(1)}_{v^{+\prime}N^{+\prime},i}(E_i)\ , \tag{10}$$

with $B_{v^{+\prime}N^{+\prime},i}(E_i)$ determined from Eq. (3). Since all these functions vanish at R_0, they constitute the closed-type basis. The basis functions y_d (with energies E_d) of the second class are set up in a similar way except that they are expanded in terms of the rovibrational functions $\chi^{(2)}_{v^+N^+}(R)$ (with energies $E^{(2)}_{v^+N^+}$) with $\chi^{(2)\prime}_{v^+N^+}(R_0)=0$:

$$y_d(E_d)=r^{-1}\sum_{v^+,N^+}\phi^{(2)}_{v^+N^+}\times\sum_{v^{+\prime},N^{+\prime}}[f^{(2)}_{v^+N^+}C^{(2)}_{v^+N^+,v^{+\prime}N^{+\prime}}-g^{(2)}_{v^+N^+}S^{(2)}_{v^+N^+,v^{+\prime}N^{+\prime}}]\times B^{(2)}_{v^{+\prime}N^{+\prime},d}(E_d)\ . \tag{11}$$

Having finite values at R_0, these will be referred to as open-type basis functions.

We have thus generated, with the help of the usual MQDT procedures for determining bound levels, two sets of multichannel basis functions. These functions, first of all, are no longer Born-Oppenheimer states. Nonadiabatic couplings, however small, have been taken into account approximately by the frame transformation procedure. Secondly, they are eigenstates of the Hamiltonian of the molecular system, i.e., $Hy_i=E_iy_i$, for instance. Within each set, these basis functions are orthogonal to each other. After normalizing all of the functions (using the usual multichannel discrete state normalization [20],

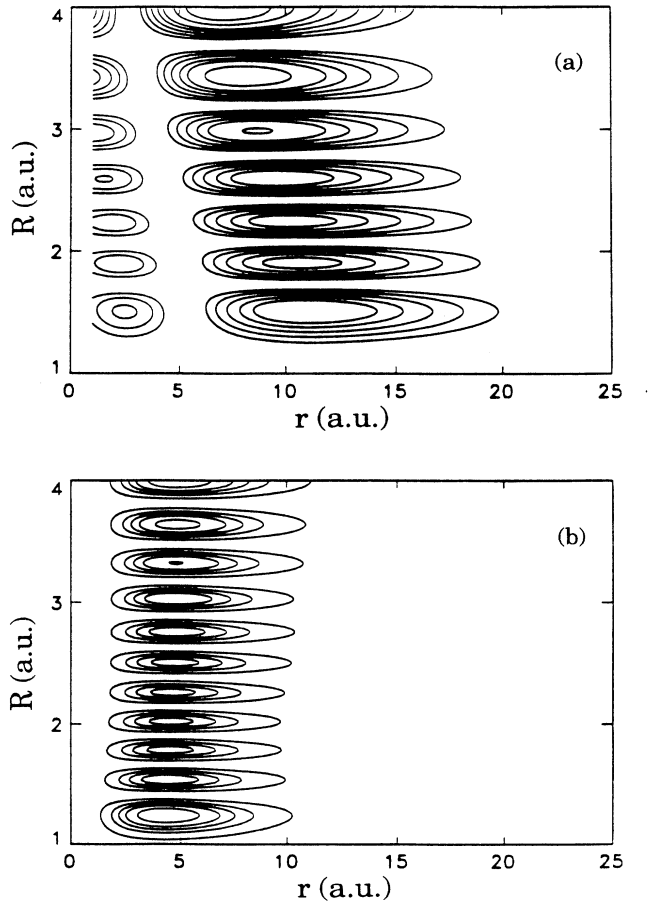

FIG. 2. Contour plots of variational basis functions of the open type used in the calculation of $v=3$ state ($R_0=4$ a.u.). (a) Basis state of $3p\sigma$ character ($v=6$); (b) basis state of $2p\pi$ character ($v=10$).

the volume integral in Eq. (9a) reduces to an orthonormality integral. Furthermore, both vanishing at large r, none of these functions will contribute to the surface integrals in the last term of Eqs. (9a) and (9b).

One can identify the energy levels in Fig. 1 as the closed-type states $\{E_i\}$ with $b=\pm\infty$. Equation (11) yields a set of open-type states $\{E_d\}$ with $b=0$. To describe the dissociation by $3p\sigma$ and $2p\pi$ states, we select from this open-type basis set two states, one for each symmetry near the energy of interest. Figure 2 shows contour plots of the two open-type basis functions used to evaluate the predissociation level $v=3$. The fact that the nodal lines are nearly parallel to the r and R axes indicates that the adiabatic approximation is still quite justified. One can identify the states as the $v=6$ and 10 "box" levels ($R_0=4$ a.u.) of the $3p\sigma$ and $2p\pi$ states, respectively. However, it is the small nonadiabatic coupling which is not perceptible in the figure that gives rise to the predissociation. The closed-type states $\{y_i\}$, together with the two open-type states y_d, constitute our variational basis. These two sets of states will be coupled in the R-matrix calculation ($\Gamma_{id}\neq 0$ when $i=3p\pi$ and $d=3p\sigma$, for instance) leading to the predissociation.

The $\underline{\Gamma}$ and the $\underline{\Lambda}$ matrices are evaluated as follows. We first expand the open-type basis function y_d in terms of the dissociative electronic states $\phi_{n\Lambda}$ ($n\Lambda=3p\sigma,2p\pi$) on the surface $R=R_0$. This is valid since we assumed the validity of the Born-Oppenheimer approximation beyond $R=R_0$ [cf. Eq. (4)]. The projection coefficients are given by the following expression:

$$a_{n\Lambda,d}=\int_{\Sigma_R}\phi^*_{n\Lambda}y_d\,d\sigma_R$$
$$=\frac{2}{\pi}\mathcal{N}_{n\Lambda}\sum_{v^+N^+}\frac{\chi^{(2)}_{v^+N^+}(R_0)U^{(lJ)}_{N^+\Lambda}}{2[\varepsilon_\Lambda(R_0)-(E_d-E^{(2)}_{v^+N^+})]}$$
$$\times\sum_{v^{+\prime}N^{+\prime}}\{\cos[\pi\mu_\Lambda(R_0)]S^{(2)}_{v^+N^+,v^{+\prime}N^{+\prime}}-\sin[\pi\mu_\Lambda(R_0)]C^{(2)}_{v^+N^+,v^{+\prime}N^{+\prime}}\}B^{(2)}_{v^{+\prime}N^{+\prime},d}\ . \tag{12}$$

In deriving Eq. (12) we have made use of the fact that the dissociative electronic Rydberg state $\phi_{n\Lambda}$ can be expressed at large r as

$$\phi_{n\Lambda}=\varphi^{(\varepsilon)}_{\Lambda^+}X^{(l\Lambda)}_{JM}(\hat{r}',\hat{R})$$
$$\times\mathcal{N}_{n\Lambda}\{f_{\varepsilon_\Lambda}(r)\cos[\pi\mu_\Lambda(R)]$$
$$-g_{\varepsilon_\Lambda}(r)\sin[\pi\mu_\Lambda(R)]\}\ . \tag{13}$$

In this expression, $X^{(l\Lambda)}_{JM}(\hat{r}',\hat{R})$ is the eigenfunction of the total angular momentum of the system and of the electronic angular momentum component along the internuclear axis Λ. It is related to $\Phi^{(lN^+)}_{JM}$ by a geometric rotational frame transformation $X^{(l\Lambda)}_{JM}=\sum_{N^+}\Phi^{(lN^+)}_{JM}U^{(lJ)}_{N^+\Lambda}$. The quantum defect $\mu_\Lambda(R)$ and the electronic energy $\varepsilon_{n\Lambda}(R)$ are related by the R-dependent Rydberg formula:

$$\varepsilon_{n\Lambda}(R)=U_{n\Lambda}(R)-U^+(R)=-\frac{Z^2}{2[n-\mu_\Lambda(R)]}\ , \tag{14}$$

where $U_{n\Lambda}(R)$ and $U^+(R)$ are potential-energy curves of H_2 and H_2^+. $\mathcal{N}_{n\Lambda}=(n-\mu_\Lambda)^{-3/2}$ is the normalization constant of the electronic state $\phi_{n\Lambda}$ [2]. These electronic states vanish at $r=r_2$, and the Wronskian of f and g equals $2/\pi$. A similar expression can be obtained when we project $\partial y_i/\partial R$ onto $\phi_{n\Lambda}$ at R_0:

$$a_{n\Lambda,i}=\int_{\Sigma_R}\phi^*_{n\Lambda}\frac{\partial y_i}{\partial R}d\sigma_R\ . \tag{12'}$$

In terms of the coefficients $a_{n\Lambda,i}$, and $a_{n\Lambda,d}$, and with the specific boundary conditions at $R=R_0$ chosen for the functions y_i and y_d, the $\underline{\Gamma}$ and $\underline{\Lambda}$ matrices reduce to the following simple forms:

$$\Gamma_{ii'}=2(E-E_i)\delta_{ii'}\ ,$$
$$\Gamma_{id}=\Gamma_{di}=-\frac{E-E_d}{E_i-E_d}\sum_{n,\Lambda}a_{n\Lambda,d}a_{n\Lambda,i}\ , \tag{15a}$$
$$\Gamma_{dd'}=2(E-E_d)\delta_{dd'}\ ,$$
$$\Lambda_{ii'}=0\ ,$$
$$\Lambda_{id}=\Lambda_{di}=0\ , \tag{15b}$$
$$\Lambda_{dd'}=\sum_{n,\Lambda}a_{n\Lambda,d}a_{n\Lambda,d'}\ .$$

At each total energy E, the generalized eigenvalue system Eq. (8) yields a complete set of R-matrix eigenstates which are superpositions of our variational basis $\Psi_\beta=\sum_i y_i c_{i\beta}+\sum_d y_d c_{d\beta}$ and have constant logarithmic derivatives b_β at $R=R_0$. The wave function Eq. (4) of the system at large R can then be matched to these R-matrix eigenstates on the surface $R=R_0$. The result is

$$I_{n\Lambda,\beta}=[G'_{n\Lambda}(R_0)+b_\beta G_{n\Lambda}(R_0)]\sum_d a_{n\Lambda,d}c_{d\beta}\ , \tag{16a}$$

$$J_{n\Lambda,\beta}=[F'_{n\Lambda}(R_0)+b_\beta F_{n\Lambda}(R_0)]\sum_d a_{n\Lambda,d}c_{d\beta}\ . \tag{16b}$$

The eigenvalues of the reaction matrix $\underline{J}\,\underline{I}^{-1}$, $\tan\pi\delta_\rho$, give the eigenphases from which the positions and widths of predissociation levels are extracted.

V. RESULTS AND DISCUSSION

In our calculations we have used the quantum-defect curve for $\Lambda=0$ ($4p\sigma B''$ state) and $\Lambda=1$ ($3p\pi D$ state) from Jungen and Atabek [8]. We typically include about

25 closed-type basis functions y_i. They are selected according to their energies E_i which cover a range in the vicinity of the $3p\pi$ level v (cf. Fig. 1). We also include two open-type basis functions y_d (one of $3p\sigma$ character and the other of $2p\pi$ character). The values $N^+=1$ and 3 are taken in the expansion in Eqs. (10) and (11) as required by the angular momentum coupling for a p electron when $J=2$. Up to 30 vibrational basis functions (for each N^+) are used in the expansion. We have varied the R-matrix radius R_0 in order to ascertain that the calculated level positions and widths do not depend on it. The largest value used in the calculations is $R_0=6.8$ a.u. For the levels $3p\pi$, $v=3-6$ all ionization channels are closed (cf. Fig. 1). For $v\geq 7$ the $3p\pi D$ state is also subject to weak preionization; however, we have neglected this decay channel by simply eliminating all open ionization channels v^+N^+ from the basis. In the course of the calculations we found that for the lowest predissociating $3p\pi$ level, $v=3$, convergence was not obtained as easily as for the higher levels v. The reason is that this level is very close to the dissociation limit $H(1s)+H(2s,2p)$.

We have evaluated the predissociation level positions and widths for $v=3-11$ of the $3p\pi$ state for $J=2$. As an example, Fig. 3 shows the eigenphase sum for the $v=3$ level along with the partial eigenphases in the $3p\sigma$ and $2p\pi$ channels. It is seen that as a function of energy, the eigenphase in the $3p\sigma$ channel displays a resonance profile, whereas that in the $2p\pi$ channel does not. This behavior confirms that the coupling to the $2p\pi$ state is much weaker than that to the $3p\sigma$ channel, and the resonance arises purely from the predissociation to the $3p\sigma$ continuum state. By fitting the resulting resonance profile of the eigenphase sum to the Breit-Wigner resonance expression we finally extracted the level position and width for each level.

Table I lists the experimental energies E_{expt} of the $v=3-11$ levels of the $3p\pi D\ ^1\Pi_u^+$ state with $J=2$ according to Takezawa [22] along with our calculated resonance energies E_{res} and widths Γ_{res}. Also given are the level shifts ΔE induced by predissociation. These correspond to the difference between the resonance energies and the energies of the hypothetical discrete levels $3p\pi,v$ calculated from Eq. (3) by restricting the vibrational basis to values $v^+\leq v+3$, whereby the dissociative $2p\pi$ and $3p\sigma$ levels are eliminated (cf. Fig. 1). Notice that these hypothetical discrete levels have no strict physical meanings; in fact, unlike the predissociation calculations, they depend somewhat on the numbers of the basis functions included. Nevertheless, it can be seen that the level shifts are much smaller than the widths. This indicates that the effective coupling leading to predissociation depends only weakly on energy. Note also that Takezawa has not made a proper line profile analysis, while Glass-Maujean, Breton, and Guyon do not give the resonance positions. Therefore, the energies E_{expt} and E_{res} in Table I are not strictly comparable.

TABLE I. Predissociation level positions and linewidths (cm^{-1}) for $3p\pi D\ ^1\Pi_u^+$ state ($J=2$).

v	E_{expt}	E_{res}	ΔE	Γ_{res}
3	119 320.5	119 318.5	−1.7	14.1
4	121 160.5	121 156.0	1.6	14.2
5	122 879.2	122 876.5	−2.1	14.1
6	124 476.4	124 475.2	3.0	11.9
7	125 959.3	125 956.5	−2.7	11.3
8	127 321.0	127 319.1	−1.4	10.3
9	128 563.4	128 561.0	−2.8	10.0
10	129 681.2	129 679.0	−0.6	9.1
11	130 673.1	130 669.5	0.1	8.8

In Fig. 4 we compare our calculated level widths for

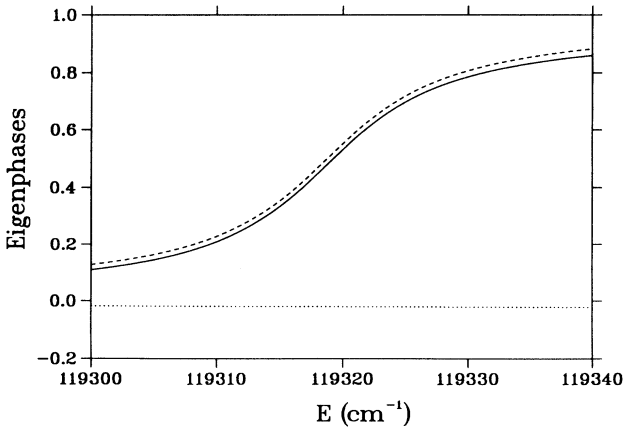

FIG. 3. Eigenphase sum (solid line) and partial eigenphases in the $3p\sigma$ channel (dashed line) and the $2p\pi$ channel (dotted line) as functions of energy for the $3p\pi D\ ^1\Pi_u^+$ ($v=3, J=2$) level.

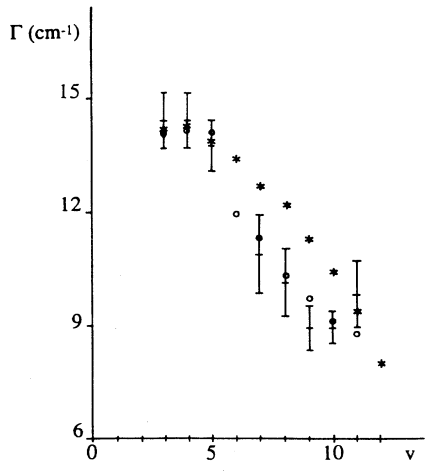

FIG. 4. Predissociation widths Γ of the $J=2$ levels of the $3p\pi D\ ^1\Pi_u^+$ state plotted as a function of the vibrational quantum number v. Asterisks refer to the theoretical Fermi "golden-rule" calculations of Julienne [18]; circles are our MQDT calculations; error bars represent the experimental measurements of Glass-Maujean, Breton, and Guyon [7].

$v=3-11$ with the experimental results of Glass-Maujean, Breton, and Guyon [7] and the theoretical results of Julienne [18]. It can be seen that while the previous Fermi "golden-rule" calculations gave the correct overall behavior of the widths as function of vibrational quantum number, our present results account now qualitatively for the details of the observations up to $v=11$. The reason for the overall decreasing trend of the width with v is that the Coriolis coupling is roughly proportional to $1/R^2$ [18]. The maximum deviations between our values and those of Julienne are of the order of about 15%. They arise because our calculations include higher-order interactions affecting the Rydberg states, as has been pointed out above. For instance, Fig. 1 shows that for $v=6-8$ the $3p\pi$ levels are in close resonance with the levels $v=4-6$ of the $4p\sigma B''$ state, which tends towards the same dissociation limit. It is indeed in this region that the "golden-rule" results deviate most markedly from the MQDT results.

For $v=11$ the experimental level width starts to rise again, but this rise is reproduced neither by the previous calculations of Julienne nor by ours. Glass-Maujean, Breton, and Guyon [7] conjectured that this rise may be due to the coupling of the $3p\pi$ and $4p\sigma$ states. Interacting with the $4f\sigma$ state, the $4p\sigma$ state has in fact a double-minimum potential curve which intersects $3p\pi$ near $R\simeq 5.5$ a.u. The outer turning points of the $3p\pi, v\geq 10$ levels are near the intersection point. These levels then have some amplitude in the potential barrier (not shown in Fig. 1) and thus reach farther out. The vibronic coupling at large internuclear distances would thus be responsible for the additional broadening of the $v=11$ level. The reason that we are not able to account for this effect at large v is that the information about the interaction of $3p\pi$ and $4p\sigma$ is not included in our quantum-defect function $\mu_\Lambda(R)$ (cf. Ref. [8] for details). Put another way, the potential-energy curve $4p\sigma$ generated from our quantum-defect function with the Rydberg equation (14) does not intersect the $3p\pi$ curve. Another reason for the discrepancy may be the fact that the $3p\pi, v=11$ level lies close to the $v^+=3$ ionization threshold and is embedded in the dense Rydberg manifold associated with that limit.

Above the ionization threshold $H_2^+(v^+=0)+e$, ionization and dissociation are in competition. It is the goal of our future work to describe the complicated processes in this region following the same lines as given in this work. We are also aiming at incorporating processes involving electronic channel interactions in addition to the rovibrational channel interactions considered here. The resulting "grand" treatment will be able to account for a great variety of decay phenomena observed in small molecules.

ACKNOWLEDGMENTS

One of us (H.G.) would like to thank the French Ministry of Foreign Affairs for support. This work was supported in part by the National Science Foundation.

[1] I. Nenner and J. A. Beswick, in *Handbook on Synchrotron Radiation,* edited by G. V. Marr (Elsevier, New York, 1987), Vol. 2, p. 355.
[2] Ch. Jungen, Phys. Rev. Lett. **53**, 2394 (1984).
[3] I. F. Schneider, O. Dulieu, and A. Giusti-Suzor, J. Phys. B **24**, L289 (1991); S. L. Guberman and A. Giusti-Suzor, J. Chem. Phys. **95**, 2602 (1991); O. Dulieu, A. Giusti-Suzor, and F. Masnou-Seeuws, J. Phys. B **24**, 4391 (1991).
[4] J. P. Gauyacq, J. Phys. B **16**, 4049 (1983).
[5] G. Herzberg and Ch. Jungen, J. Mol. Spectrosc. **41**, 425 (1972).
[6] P. M. Dehmer and W. A. Chupka, J. Chem. Phys. **65**, 2243 (1976); S. T. Pratt, P. M. Dehmer, and J. L. Dehmer, *ibid.* **86**, 1727 (1987).
[7] M. Glass-Maujean, J. Breton, and P. M. Guyon, Chem. Phys. Lett. **63**, 591 (1979); Z. Phys. D **5**, 189 (1987).
[8] Ch. Jungen and O. Atabek, J. Chem. Phys. **66**, 5584 (1977); Ch. Jungen and D. Dill, *ibid.* **73**, 3338 (1980).
[9] G. Raseev, J. Phys. B **18**, 423 (1984).
[10] S. Kander and M. Shapiro, J. Phys. B **16**, L655 (1983).
[11] C. Mündel, M. Berman, and W. Domcke, Phys. Rev. A **32**, 181 (1985).
[12] M. J. Seaton, Rep. Prog. Phys. **46**, 167 (1983).
[13] C. H. Greene and Ch. Jungen, Adv. At. Mol. Phys. **21**, 51 (1985).
[14] E. S. Chang and U. Fano, Phys. Rev. A **6**, 173 (1972).
[15] A. Giusti, J. Phys. B **13**, 3867 (1980); A. Giusti-Suzor and Ch. Jungen, J. Chem. Phys. **80**, 986 (1984).
[16] F. Robicheaux, Phys. Rev. A **43**, 5946 (1991).
[17] C. H. Greene and Ch. Jungen, Phys. Rev. Lett. **55**, 1066 (1985); H. Gao and C. H. Greene, J. Chem. Phys. **91**, 3988 (1989).
[18] P. S. Julienne, Chem. Phys. Lett. **8**, 27 (1971).
[19] G. Herzberg, in *Topics in Modern Physics—A Tribute to Edward U. Condon,* edited by W. E. Brittin and H. Odabasi (Colorado Associated University Press, Boulder, 1971), p. 191.
[20] U. Fano and C. M. Lee, Phys. Rev. Lett. **31**, 1573 (1973).
[21] C. H. Greene, Phys. Rev. A **28**, 2209 (1983); H. Le Rouzo and G. Raseev, *ibid.* **29**, 1214 (1984).
[22] S. Takezawa, J. Chem. Phys. **52**, 2575 (1970).